Low-temperature internal quantum efficiency of GaInN/GaN quantum wells under steady-state conditions

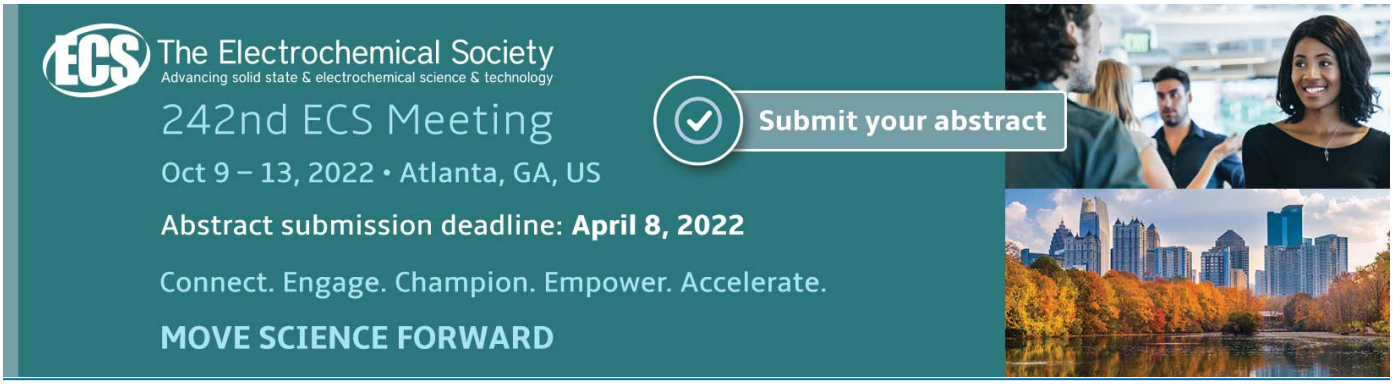

OPEN ACCESS
IOP Publishing
Semiconductor Science and Technology
Semicond. Sci. Technol. **37** (2022) 035017 (10pp)
https://doi.org/10.1088/1361-6641/ac4b89

Low-temperature internal quantum efficiency of GaInN/GaN quantum wells under steady-state conditions

Shawutijiang Sidikejiang[1,2,*], Philipp Henning[1,2], Philipp Horenburg[1,2], Heiko Bremers[1,2], Uwe Rossow[1,2], Dirk Menzel[3] and Andreas Hangleiter[1,2]

[1] Institut für Angewandte Physik, Technische Universität Braunschweig, Mendelssohnstr. 2, 38106 Braunschweig, Germany
[2] Laboratory for Emerging Nanometrology, Technische Universität Braunschweig, Langer Kamp 6a, 38106 Braunschweig, Germany
[3] Institut für Physik der Kondensierten Materie, Technische Universität Braunschweig, Mendelssohnstr. 3, 38106 Braunschweig, Germany

E-mail: s.sidikejiang@tu-braunschweig.de

Received 14 October 2021, revised 30 December 2021
Accepted for publication 14 January 2022
Published 31 January 2022

Abstract

We compare the low-temperature photoluminescence (PL) intensities of a range of GaInN/GaN quantum well (QW) structures under identical excitation conditions, mounting the samples side by side. Normalizing the measured intensity to the absorbed power density in the QWs, we find that low-temperature PL efficiencies of several samples, which show close to 100% internal quantum efficiency (IQE) in time-resolved PL, saturate at nearly an identical value. Of course, this is strong indicative of being 100% IQE at low temperature for those efficient samples. Using the low-temperature PL efficiency as a 'Reference', on the other hand, we observe not only the effects of temperature-independent non-radiative losses on the low-temperature IQE, but also are able to determine the IQE of arbitrary samples on an absolute scale. Furthermore, we prove the experimental results by comparing the low-temperature efficiencies of a sample with an initial 100% IQE after intentionally introducing structural defects with argon-implantation.

Keywords: LEDs, internal quantum efficiency, GaInN/GaN quantum wells, PL efficiency

(Some figures may appear in colour only in the online journal)

1. Introduction

Since the first commercial GaN-based blue light emitting diodes (LEDs) by Nakamura *et al* [1], III-nitride-based LEDs have been extensively developed for targeting solid-state lighting applications. By now, the most of the conventional light sources have been replaced by the more efficient GaN-based ones whose external quantum efficiency (EQE) is of the order of 80% [2]. However, a significant drop of efficiency has been reported for longer emission wavelength, the so-called green gap [3, 4]. Several different reasons have been outlined to explain the limitation regarding the green gap [5–8] but the mechanism responsible for this behaviour is still under debate. To gain a better understanding of the limiting factors, an accurate assessment of the efficiency is highly important.

The performance of GaInN/GaN quantum well (QW) structures can be assessed by determining their internal quantum efficiency (IQE), which is the ratio of radiative recombination rate and the total recombination rate (radiative plus

* Author to whom any correspondence should be addressed.

non-radiative rates). While the IQE cannot be measured directly, the EQE of electrically driven LEDs can be measured using an integrating sphere. The EQE (η_{ext}) is given by the ratio of emitted photons and injected electrons, i.e. the IQE (η_{int}), the light extraction efficiency (η_{extr}) and the current injection efficiency (η_{inj})

$$\eta_{\text{ext}} = \eta_{\text{extr}} \times \eta_{\text{int}} \times \eta_{\text{inj}}. \quad (1)$$

The IQE (η_{int}) can be determined from the measured η_{ext} using equation (1), if η_{extr} and η_{inj} are known. Actually, the measured EQE provides a lower bound to the IQE, as both η_{extr} and η_{inj} are smaller than unity.

It is common to use photoluminescence (PL) measurements to determine the IQE. Normalizing the temperature-dependent PL intensity to the maximum PL intensity at low temperature, and to the respective excitation power, could give the temperature-dependent IQE [9]. This estimation is based on the assumption of an IQE of 100% at low temperatures, which can be justified when thermally activated, defect-related non-radiative recombination gets suppressed. However, besides thermal activation, non-radiative recombination could involve tunnelling processes even in the low-temperature limit, exhibiting no dependence on temperature [10–12]. This potentially reduces the low-temperature IQE, adding an additional unknown error margin. Thus, in face of such unknown uncertainty in experimental practice, this assumption needs an experimental verification.

Several measurement techniques have been proposed to determine the IQE on an absolute scale. In order to assess non-radiative losses, photo-acoustic spectroscopy and bolometric measurements were proposed to measure the heat produced by non-radiative recombination processes [13, 14]. Kazunobu *et al* [15] have proposed omnidirectional PL spectroscopy to quantify the absolute IQE using an integrating sphere. Recently, an experimental verification of 100% absolute IQE at low temperatures for GaInN/GaN QW samples has been demonstrated using time-resolved PL (TRPL) [16]. Nevertheless, temperature-dependent PL measurements remain a practical means to evaluate the IQE with regard to fundamental properties of QW structures.

In the present work, we measured the low-temperature PL intensities of a range of QW samples under otherwise identical conditions, mounting the samples side by side. Similar structures have also been studied using TRPL [16], where a unity IQE at low temperature has been experimentally demonstrated. We made a comparison of the low-temperature PL efficiency, which we define as the ratio of the integrated PL intensity and the absorbed power density in the QW. It is important to note that the term 'PL efficiency' should not be confused with the IQE, which has the well-known definition of numbers of photons generated per absorbed photon in the QW. The PL efficiency is a quantity that is used here for comparison of the samples mounted side by side. We find that the PL efficiencies of several samples, which show 100% IQE at low-temperature in TRPL measurements, are identical under steady-state PL excitation. On the other hand, for samples with a reduced low-temperature IQE observed in TRPL, the PL efficiencies saturate at significantly lower values. Clearly, the results not only allow us to confirm the assumption of unity IQE at low temperatures for those efficient samples, but also to estimate the absolute IQE of samples with lower efficiency by a direct comparison. In addition, a significant reduction of the low-temperature IQE is observed for samples with Ar ion implantation induced point defects in the QWs.

2. Experimental

The samples under investigation (labelled A, B, C, D, E, F, H, and G) have been prepared by low pressure metal-organic vapour phase epitaxy (Aixtron AIX200RF) on *c*-plane sapphire substrates. After a 2 μm GaN buffer layer, single (A, B, F, G, and H) or multiple ($\times$5) (C, D, and F) GaInN/GaN QW structures were grown at temperatures between 740 °C and 800 °C followed by a GaN capping layer with a thickness of about 50 nm. The active regions of the samples were grown at different temperatures and with different growth time, thus indium composition and thickness of the QW are different. High resolution x-ray diffraction (HRXRD) was used to assess structural parameters such as layer thickness and composition. As HRXRD can only be done for multiple quantum wells (MQWs), identical growth conditions are used to estimate indium content and thickness of the single quantum well (SQW). A summary of the structural analysis and the emission features of the samples are given in table 1. In order to investigate the impact of non-radiative recombination due to Ar implantation on the absolute IQE of samples, we introduced intentional point defects in sample A by Ar ion implantation with different doses (samples F, G, H). Further details about the Ar implantation can be found elsewhere [17]. Note that the PL peak position of implanted sample G with a dose of 3×10^{11} cm^{-2} is shifted to a higher energy of about 33 meV (e.g. $\sim$3 nm) with respect to the unimplanted sample A, see table 1. This behaviour can be interpreted as being indicative of generation of additional background charge carriers by implantation-induced defects, corresponding to stronger screening of the piezoelectric field by the background charge carriers.

The PL measurements were carried out using a diode laser with an excitation wavelength of 376 nm. The laser beam is focused to a spot of about 100 μm. The PL signal was analyzed with a 0.32 m spectrometer equipped with a CCD detector. For low-temperature PL measurements, samples were mounted side by side in a continuous-flow helium cryostat and maintained at a temperature of $T_0 = 15$ K during the measurements. Resonant PL excitation was performed with a maximum incident power density of 46 W cm^{-2}. The incident power was varied by a calibrated motorized neutral density filter wheel. In order to minimize the measurement uncertainty due to inhomogeneities, six PL spectra for each power level are recorded from different spots on the surface for further analysis. The temperature-dependent IQE measurements were performed in a temperature range between 15 and 300 K.

Table 1. Overview of the samples (S) under investigation, with QW thickness (L_{QW}), indium composition (x_{In}) as well as number of QWs (n_{QW}). Emission energy ($E_{300\ K}$), linewidth of the spectra ($w_{300\ K}$), low-temperature IQE determined by TRPL (η_{TRPL}), PL efficiency (PL) at an absorbed power density of about 0.03 W cm^{-2} at 15 K, as well as implantation dose (N) for Ar implanted samples are listed. As the Ar-implanted samples do not show a synchronous rise of the effective and radiative lifetimes at low temperatures, it is not possible to determine the absolute low-temparture η_{TRPL}.

S	L_{QW} (nm)	x_{In}	n_{QW}	$E_{300\ K}$ (eV)	$w_{300\ K}$ (meV)	η_{TRPL} (%)	PL (arb. u.)	N (cm^{-2})
A	1.35 ± 0.14	20 ± 1	$\times 1$	2.79	149.4	99.91 ± 5	7.4 ± 2	—
B	1.06 ± 0.11	33 ± 3	$\times 1$	2.66	164.6	99.99 ± 1	7.4 ± 4	—
C	1.27 ± 0.13	10 ± 1	$\times 5$	2.96	157.4	99.93 ± 2	7.3 ± 3	—
D	1.45 ± 0.11	30 ± 2	$\times 5$	2.38	264.1	65 ± 12	5.0 ± 3	—
E	1.19 ± 0.10	32 ± 3	$\times 5$	2.34	118.5	84 ± 15	4.2 ± 4	—
F	1.35 ± 0.14	20 ± 1	$\times 1$	2.79	172.2	—	5.0 ± 2	1×10^{11}
G	1.35 ± 0.14	20 ± 1	$\times 1$	2.82	242.1	—	4.7 ± 1	3×10^{11}
H	1.35 ± 0.14	20 ± 1	$\times 1$	—	—	—	1.4 ± 3	1×10^{12}

Sample H does not show luminescence at room temperature due to a large defect density.

3. Results and discussion

The IQE is essentially a key figure of merit to assess the performance of GaInN/GaN QW structures and is generally given by the ratio of the radiative recombination rate (R_r) and the total recombination rate ($R_r + R_{nr}$)

$$\eta_{int} = \frac{R_r}{R_r + R_{nr}} = \frac{\frac{1}{\tau_r}}{\frac{1}{\tau_r} + \frac{1}{\tau_{nr}}} = \frac{\tau_{eff}}{\tau_r}, \tag{2}$$

where τ_{eff}, τ_r, and τ_{nr} are effective, radiative, and non-radiative lifetimes. Thus, an absolute experimental assessment of the IQE would be possible if one could measure those carrier lifetimes. For a nondegenerate semiconductor under low-excitation conditions, the temperature dependence of the radiative lifetime τ_r can be related to the dimensionality D of the system, in which the charge carriers are confined [18]

$$\tau_r \propto T^{D/2}, \tag{3}$$

according the above relation, a constant radiative lifetime can be expected in the low temperature limit due to localization of the charge carriers (or excitons) at certain potential minima, i.e. likely zero-dimensional states in the QW [19, 20]. With increasing temperature, a linear increase of the radiative lifetime can be predicted due to the fact that weakly localized carriers are thermally activated and freed into the 2D states. At high temperatures, non-radiative recombination processes start to come into play with thermal activation, leading to a steady increase of the radiative lifetime.

As shown in figure 1, the temperature dependence of the carrier lifetime was measured by TRPL. The measurement details as well as the derivation of the carrier lifetimes from the PL transient signal after a pulsed laser excitation are given in more details elsewhere [21]. The effective lifetime and the radiative lifetime exhibit an identical temperature dependence, where a synchronous rise of both is observed up to temperatures of about 200 K. For temperatures above 225 K, the effective lifetime decreases monotonically and is dominated by non-radiative processes. The synchronous rise of the effective and radiative lifetimes at low temperatures is a strong indication that the effective carrier decay time is dominated only by radiative recombination at low temperatures. Thus, an IQE of nearly 100% can be estimated for the sample A, according to (2). Recently, we have demonstrated an experimental verification of a unity IQE at low-temperature for similar GaInN/GaN QWs using TRPL [16], and an absolute IQE value is obtained by simultaneously fitting the model functions to the temperature dependence of carrier lifetimes, separately. A definite IQE of $(99.91 \pm 0.05)\%$ is quantified for the sample A using the same simultaneous fitting procedure, as shown in figure 1. Nonetheless, not all samples investigated in TRPL show a significant range of synchronous rise of the effective and radiative lifetime with temperature, and a strong deviation between the effective and the radiative lifetime is observed already at cryogenic temperatures for some samples. In such cases, the assumption of an unity IQE at low temperature may not hold true. Then, the only way to estimate the IQE of those samples could be a direct comparison of the low-temperature PL intensity to one of those showing 100% IQE at low temperature.

The comparison of the PL intensities of the samples was carried out at 15 K. The evaluation of the PL efficiency is conducted by considering the cw-PL excitation as steady state, i.e. that the total recombination rate R_{tot} is equal to the generation rate G. In turn, the generation rate is proportional to the absorbed power P_{abs} in the QWs. Resonant excitation conditions in the QWs make sure that the absorption only takes place in the GaInN QW layer, hence carriers generated in the GaN barrier layer can be neglected. The low-temperature integrated PL intensity I_{PL} is proportional to the radiative recombination rate $I_{PL} \propto R_r$, and the PL efficiency (η_{PL}) can be written as

$$\eta_{PL} = \frac{R_r}{R_{tot}} = \frac{R_r}{G} \propto \frac{I_{PL}}{P_{abs}}, \tag{4}$$

In case of small absorption, as for thin QWs, the expression in (4) can be further approximated as

$$\eta_{PL} \propto \frac{I_{PL}}{P_{abs}} = \frac{I_{PL}}{P_{in} \times \alpha(\lambda) \times n_{QW} \times L_z}, \tag{5}$$

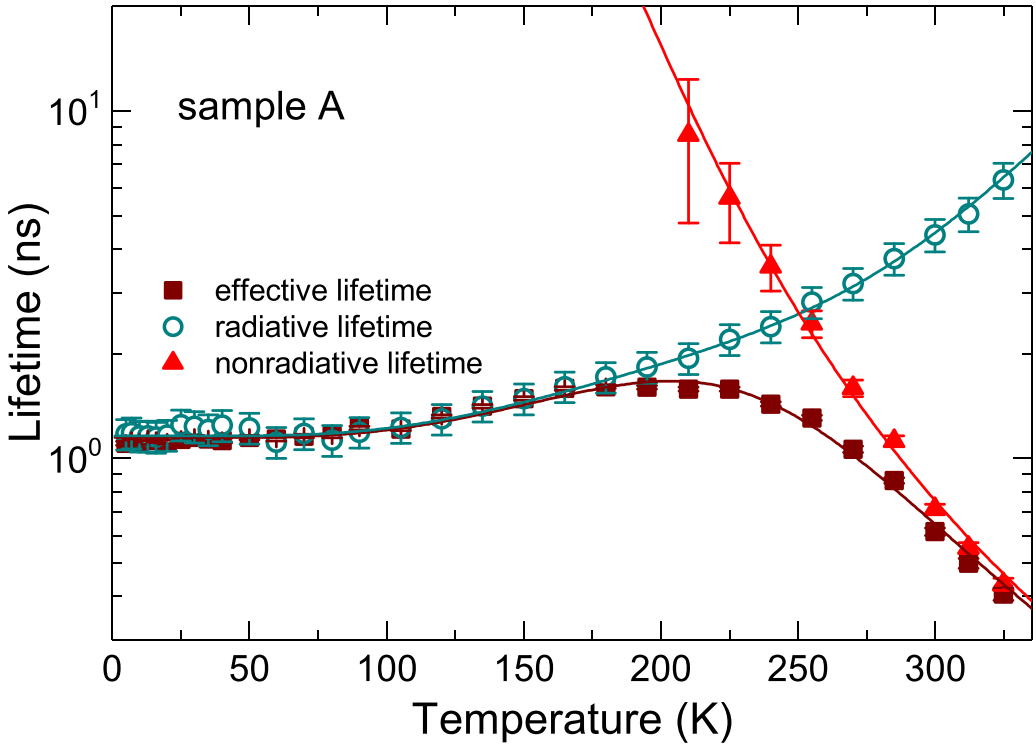

Figure 1. Temperature dependence of the effective lifetime, the radiative lifetime, and the non-radiative lifetime of sample A. A synchronous rise of the effective lifetime with the radiative lifetime is visible up to temperatures of about 200 K. The measured effective and radiative lifetimes were fitted with the model functions described in [16] to obtain the ratio between the radiative and non-radiative lifetimes at low-temperature. Thus, an absolute low-temperature IQE of $(99.91 \pm 0.05)\%$ can be determined.

where P_{in}, $\alpha(\lambda)$, n_{QW} and L_z are incident power density, QW absorption coefficient, number of QWs and thickness of QWs, respectively. Please note that in this way we compare the intensity per QW, which is necessary to be able to compare single and multiple QWs. The incident power density P_{in} is corrected for the reflectivity of 21% at the air-GaN interface using the refractive index of GaN ($n = 2.655$) at the laser wavelength [22]. Due to the small absorption in the QW, it is difficult to measure it directly. However, we can obtain the absorption at the excitation wavelength from a model calculation of the optical spectra, which is based on a self-consistent Schrödinger–Poisson solver [23]. The model calculation predicts the behaviour of GaInN/GaN laser structures quite well and an excellent agreement of calculated optical gain spectra and measured ones is achieved [23]. Therefore, we can rely on the calculated absorption within error margins of about $\pm 10\%$, which include the uncertainties associated with indium composition, QW thickness, as well as the parameters used in the calculation.

Figure 2 shows the absorbed power density per QW dependence of the PL efficiency of the samples A–E at 15 K. The PL efficiencies of samples A, B, and C converge towards an identical value of around 7.4 ± 0.3 in the low power regime. The two SQW samples (A and B) show a nearly constant PL efficiency up to the maximum absorbed power density of about 0.2 W cm^{-2}, whereas the MQW sample C shows a slight drop of efficiency towards higher absorbed power densities. It is important to note that this PL efficiency of 7.4 ± 0.3 represents the maximum value observed among all samples in this work, consistent with a close to 100% IQE obtained from TRPL, see table 1. On the other hand, the saturation of the PL efficiency for samples D and E occurs at somewhat lower values of about 5.0 ± 0.3 and 4.2 ± 0.4, respectively. The absorbed power density dependence of the PL efficiency shows similar behaviour like for samples A, B and C, staying nearly constant with increasing absorbed power density. The reduction of efficiency towards high absorbed power densities might be attributed to the efficiency droop observed both in optically and electrically pumped GaInN/GaN QW structures [24–28]. Consequently, samples D and E exhibit a low-temperature IQE lower than 100%, in qualitative agreement with the TRPL results. The side-by-side comparison of the low-temperature PL efficiencies reveals that a saturation of the PL efficiency and therefore of the IQE with respect to the absorbed power occurs at low temperatures for all samples under consideration. However, the absolute value of the IQE at low temperature (i.e. the saturation values of the PL efficiency) is lower than unity in some cases (samples D and E), indicating significant presence of non-radiative recombination. In order to be consistent with the experimental results, those non-radiative losses need to be temperature-independent, which is possible through tunnelling-assisted multi-phonon processes. The thermal energy of the system is rather small at low temperature, hence non-radiative capture processes are not possible via thermal activation. However, the quantum mechanical nature of the vibrational states of both an electron (hole)

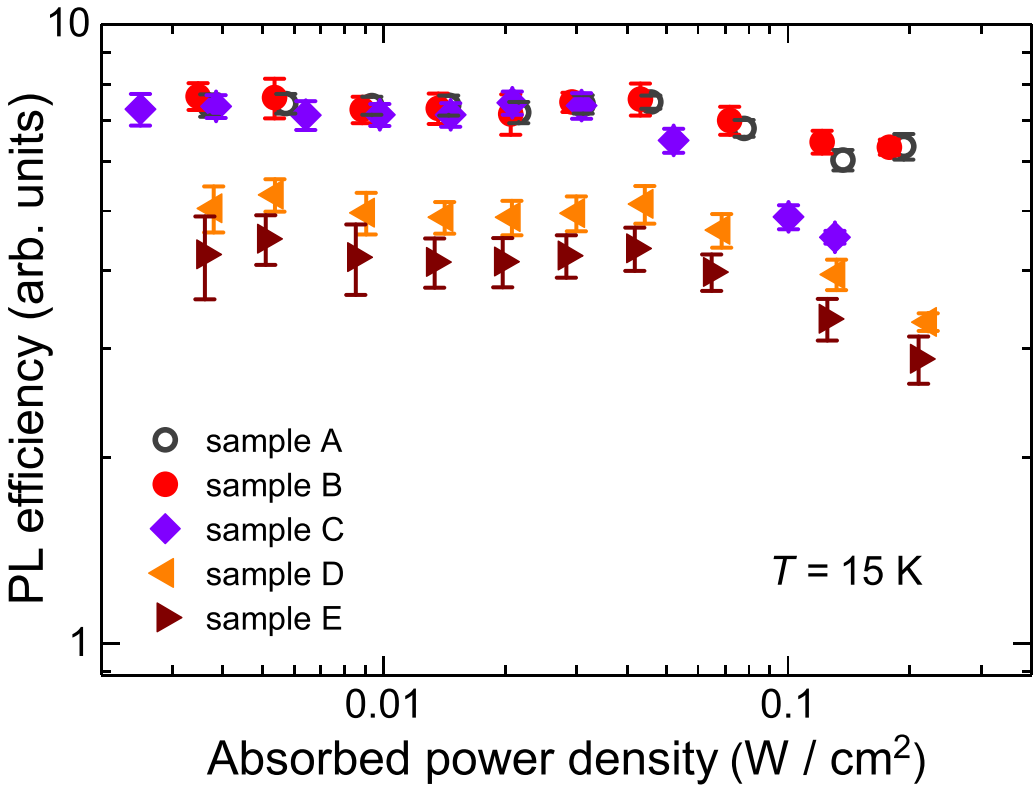

Figure 2. Side-by-side comparison of the PL efficiency as a function of absorbed power density per QW for samples A, B, C, D, and E measured at 15 K under identical measurement conditions. The evaluation of measurement data was carried out using (5).

in the bands and a trap state coupled to the system implies that there is always a non-zero probability of an overlap of those vibrational states. Thus transitions between band and trap states can be expected through the point of intersection of those vibrational states through tunnelling [11, 12]. Since the tunnelling process exhibits a rather weak temperature dependence or is independent of temperature, the non-radiative recombination rate is not necessarily vanishing in the low-temperature limit. Thus, those non-radiative losses via tunnelling-assisted multi-phonon processes are expected to lead to a significant loss of efficiency even at low temperatures.

As discussed earlier, the synchronous rise of the effective and the radiative lifetime at low temperatures is a safe indicator of vanishing non-radiative loss processes in the low temperature limit. Like sample A, samples B and C show similar temperature dependence of the effective and the radiative lifetime, where synchronous rise of the effective and the radiative lifetime is observed for a wide range of temperatures (not shown here). On the contrary, deviations between the effective and the radiative lifetime are observed for samples D and E already in the low temperature limit, thus significantly reduced low-temperature η_{TRPL} of 65 ± 12 and 85 ± 15 are estimated for the samples D and E, see table 1. Combining these experimental results, the identical low-temperature PL efficiencies of samples A, B, and C, as shown above in figure 2, can be expected since those samples show nearly 100% IQE at low-temperature in TRPL. On the other hand, the saturation of the PL efficiency at slightly lower values in the cases of D and E is not surprising, since the low-temperature effective recombination is already dominated by temperature-independent non-radiative losses, consequently, leading to even lower PL efficiency.

From the above discussion, it can be concluded that temperature-independent non-radiative losses have significant impact on the low-temperature PL efficiency. Consequently, a low-temperature normalization, which is commonly used in IQE measurements, could be problematic. Generally, the IQE can be accessed from the temperature- and power-dependent PL measurements under the assumption that non-radiative recombination processes are negligible at low temperatures, resulting in a saturation of the IQE at 100%. Normalizing the temperature-dependent PL intensity to the maximum PL intensity at low temperature, and to the respective absorbed power, could provide the temperature-dependent IQE, but on relative scale. Alternatively, the assessment of the IQE on the absolute scale can be possible by normalizing the temperature dependent PL intensities of arbitrary samples to the maximum low-temperature PL intensity of one of the efficient samples (A, B, and C), and to the respective absorbed power. As shown in figure 3, from the largely identical temperature dependence of the IQE for the samples (A, B, and C) up to a temperature of about 90 K, it can be concluded that the low-temperature IQE is indeed 100%. In contrast, the IQE of sample D deviates significantly from a unity at low temperatures, exhibiting an IQE of only ≈70% at 15 K, and dropping to close to 10% at room temperature. The direct comparison of low-temperature PL intensities of arbitrary samples to the efficient one provides

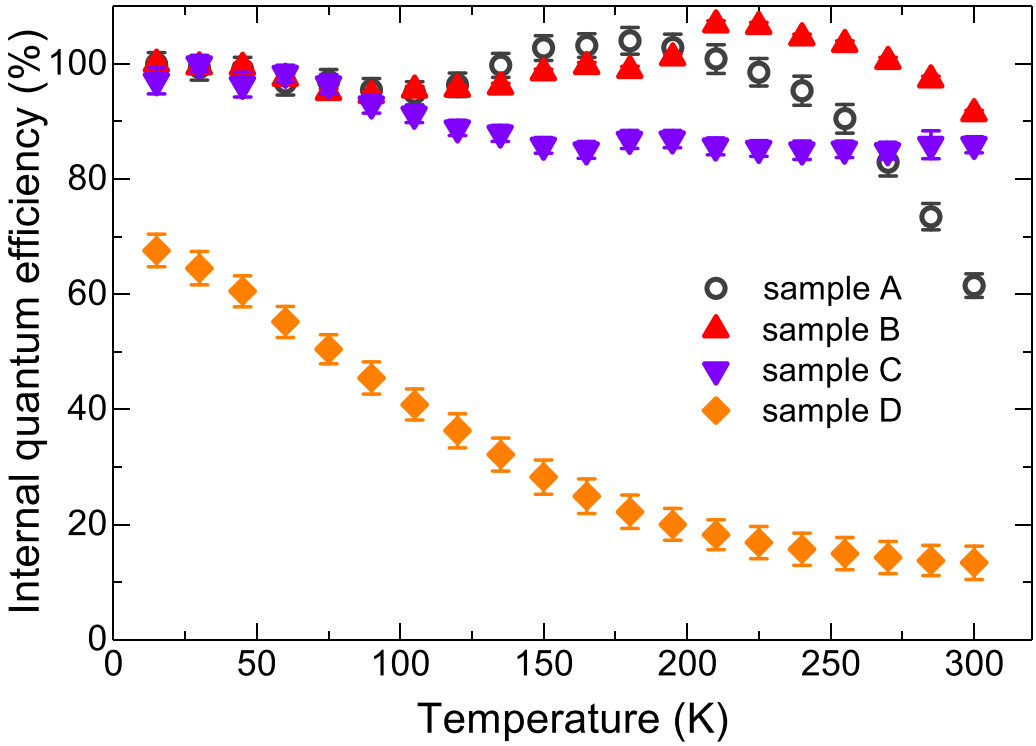

Figure 3. Temperature dependence of the IQE of samples A, B, C and D. In principle, the temperature-dependent IQE can be obtained by normalizing the temperature-dependent integrated PL intensity to the maximum PL intensity at low temperature, and to the respective absorbed power, which provides a relative IQE for the samples under consideration. In order to compare the absolute IQE of the samples, in this case, the integrated PL intensities are normalized to the maximum PL intensity of one of the efficient samples at low temperatures, and to the incident power density of 6.2 W cm^{-2}, which provides the IQE on an absolute scale.

an additional indicator of the existence of non-radiative recombination at low temperatures, and enables us to estimate the IQE on an absolute scale. Surprisingly, an increase of around 4% of the IQE is observed at around 200 K for the sample A in figure 3 (a similar trend can also be seen from the sample B), and this is likely due to the Fabry–Perot (FP) microcavity formed by the GaN/air and the GaN/sapphire interfaces. A model consisting of a normalized Gaussian peak and a FP filter function is used to qualitatively explain the observed enhancement of the IQE. The details on the FP microcavity effect can be found in the literature [29, 30].

Figure 4(a) shows the normalized Gaussian functions at several temperatures, indicating the temperature dependence of the emission wavelength shift for sample A. The dependence of the modulation depth of the FP microcavity on the wavelength is also indicated. In addition, the modulation depth depends strongly on thickness of the structure, roughness of the interference as well as damping of the reflection due to the imperfect surfaces. Since the emission wavelength of the sample shifts with temperature, which can be obtained by fitting the temperature-dependent PL spectra to the model. With increasing temperature, the emission wavelength moves into resonance with the cavity. Consequently, the constructive interference in the cavity results in a significant increase of the PL intensity. Figure 4(b) shows a monotonic increase of the integrated intensity of the model with temperature. To clearly see the effect of the FP modulation due to only the temperature shift of the wavelength on the integrated PL intensity, the other parameters in the model are set constants. The temperature dependent integrated intensity is normalized to the integrated PL at 5 K to pronounce the enhancement of 2% towards room temperature. Nonetheless, the simulated result qualitatively predicts the experimentally observed increase of 4% of the IQE towards high temperature. Strictly speaking, the above model considers only the shift of the wavelength with temperature and is likely not sufficient enough to extract the unperturbed PL intensity from the model to correct the experimentally observed IQE data, since the temperature dependence of spectral broadening as well as electron-phonon interactions might also contribute to this observed phenomenon. Besides, at this point one might ask the question of why this FP effect is not observed in other samples. In principle, the above model holds for other samples as well, since the samples have similar structures grown on a GaN buffer layer with a thickness of about 2 μm on top of sapphire substrates. However, due to the wavelength dependence of the modulation depth of the FP fringes as shown in figure 4(a). For other samples, the emission wavelengths could shift out of the resonance peak of the PF cavity. Consequently, the effect could disappear or be not pronounced to be observed.

The change of the PL efficiency by intentional creation of non-radiative centres due to Ar ion implantation into the sample A is investigated at 15 K, and the PL efficiencies of the

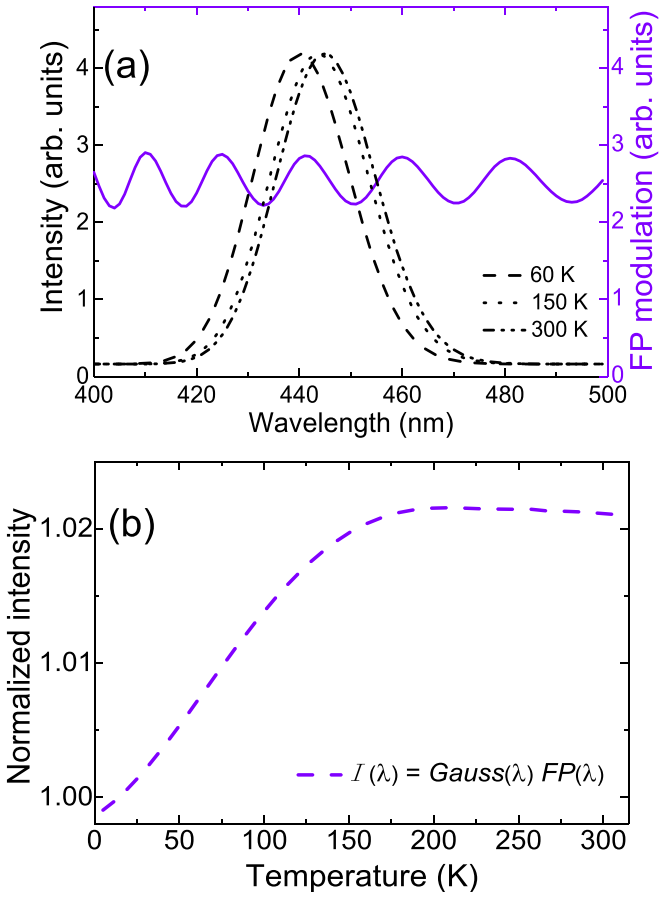

Figure 4. (a) The normalized Gaussian functions at several temperatures reproduced by using the temperature-dependent shift of the emission wavelength of the sample A. The wavelength dependence of the modulation depth of the FP fringes is shown as a solid line (blue). (b) The temperature dependence of the integrated intensity of the model function, which is normalized to the integrated intensity at 5 K. A steady increase of the PL intensity with temperature is observed due to the enhancement of the PL intensity when the emission wavelength becomes resonant with a maximum of the FP cavity.

unimplanted sample A and the Ar-implanted samples F, G, H with varying implantation doses are compared. As shown in figure 5, for the unimplanted sample A, the absorbed power density dependence of the PL efficiency shows quite identical behaviour as in figure 2, staying at a constant value with absorbed power density. In contrast, the efficiencies converge to slightly lower constant values for samples with implantation doses of 1×10^{11} and 3×10^{11} cm^{-2}. A further reduction of the PL efficiency can be observed from the sample with the highest implantation dose of 1×10^{12} cm^{-2}. The PL efficiency saturates at a significantly lower value, which is nearly a factor of eight smaller than that of the as-grown sample A. The experimental results provide supporting evidence that the Ar implantation induced defects make a significant contribution to the loss of PL efficiency even in the low temperature limit, and those defects clearly act as non-radiative recombination centres, thus enhancing the non-radiative recombination rate.

The inset in figure 5 depicts the evolution of PL efficiency with the Ar-implantation dose. The data points are normalized to the PL efficiency of the unimplanted sample A. A decrease of the PL efficiency can be seen with increasing Ar-implantation dose. For a simple model, the IQE η_{int} can be written

$$\eta_{\mathrm{int}} = \frac{\mathrm{R_r}}{\mathrm{R_r} + \mathrm{R_{nr}}} = \frac{\frac{1}{\tau_{\mathrm{r}}}}{\frac{1}{\tau_{\mathrm{r}}} + \frac{1}{\tau^0_{\mathrm{nr}}} + \frac{\mathrm{N}}{\tau^*_{\mathrm{nr}}}}, \tag{6}$$

where τ_{r} is the radiative lifetime, τ^0_{nr} is the intrinsic non-radiative lifetime, which represents a background non-radiative recombination rate at low temperatures. τ^*_{nr} is the non-radiative lifetime associated with the Ar-implantation induced defects, and N is the implantation dose. From the model, a monotonic decrease of the PL efficiency with the implantation dose is expected, since the radiative recombination can be assumed constant, and thus, the effective carrier recombination rate is only governed by the implantation induced defect-related non-radiative recombination. Nevertheless, the model could not fit data points well, this is probably not surprising since argon ion implantation can induce extended defects at higher doses [31], and a simple linear increase of non-radiative rate with implantation dose may not hold true. After all, the reduction of the PL efficiency due to the intentionally introduced defects with the Ar-implantation gives additional evidence that the structural defects promote temperature-independent non-radiative losses via tunnelling processes.

Finally, the temperature dependent IQE of the reference sample A and the argon ion implanted samples were measured at an incident power density of 6.2 W cm^{-2}. As can be seen from the figure 6, the IQE of the sample A saturates at 100% IQE at low temperatures, which is an expected behaviour, and an approximately 60% of the low-temperature IQE remains at 300 K. On the contrary, a significant decrease of the IQE of the Ar-implanted samples is visible at low temperatures, saturating only at about (69 ± 3)%, (61 ± 4)% and (19 ± 5)% for samples with Ar-implantation induced defect density of 1×10, 3×10^{11} and 1×10^{12} cm^{-2}, respectively. The IQE curves drop immediately after some temperature steps and, at room temperature, the IQE is almost close to zero for all Ar-implanted samples. These temperature-dependent IQE results show that the temperature-independent non-radiative recombination depends strongly on the defect density in the structure, and an increase of the defect density in the structure facilitates temperature-independent non-radiative recombination via tunnelling processes.

Obviously, the IQE seems to converge towards a constant value at low temperature, even though it does not reach 100%, being indicative of temperature-independent non-radiative losses. If those temperature-independent non-radiative processes are simple neglected, then the measured IQE at room temperature provides only an upper limit to the actual IQE value of the particular sample.

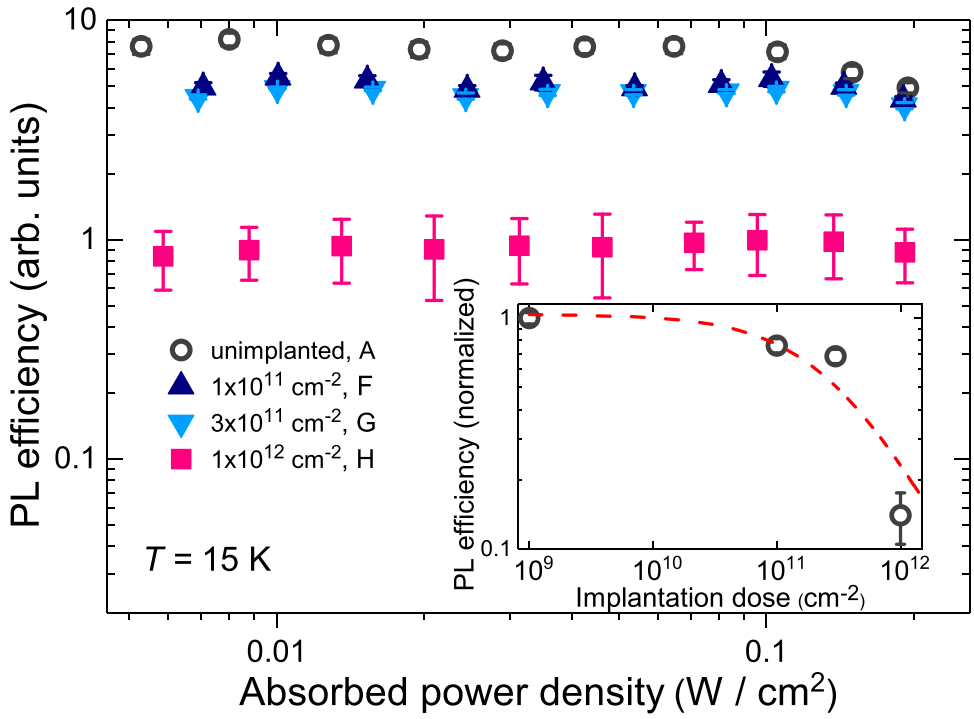

Figure 5. Comparison of the PL efficiencies of the unimplanted sample A (open circles) and the argon-implanted QW structures with implantation doses of 1×10^{11} cm^{-2} (F, up-pointing triangles), 3×10^{11} cm^{-2} (G, down-pointing triangles) and 1×10^{12} cm^{-2} (H, squares), respectively. The inset shows the variation of the normalized PL efficiency with different implantation doses at an absorbed power density of about 0.1 W cm^{-2} and the dashed line represents a fit to the measurement points as described in the text. For the unimplanted sample A, an implantation dose of 1×10^{9} cm^{-2} is assumed.

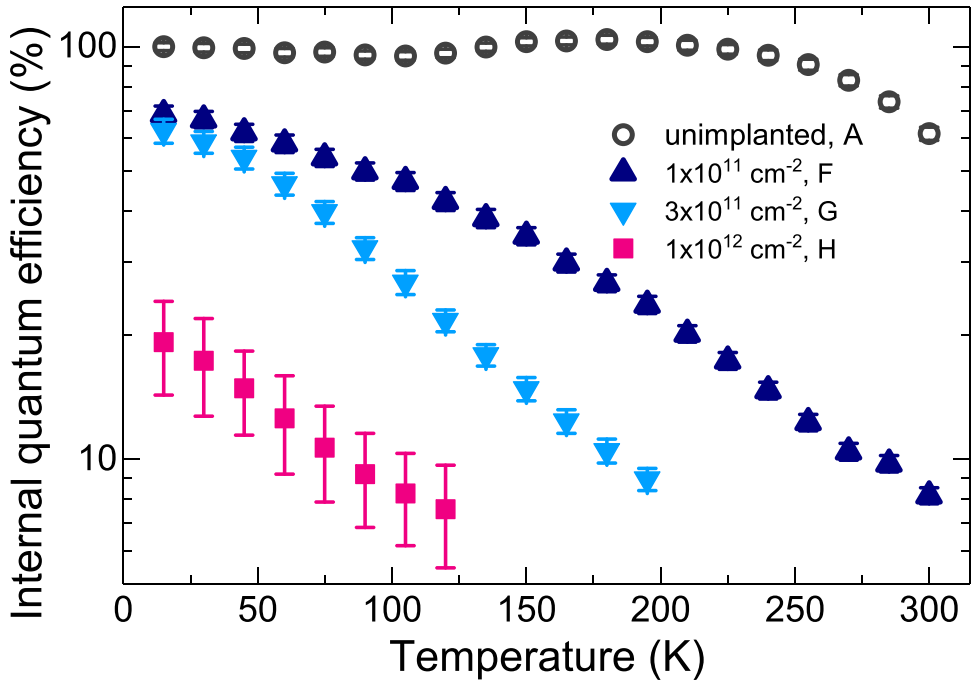

Figure 6. Temperature dependence of the IQE of the unimplanted sample A and the Ar-implanted samples with varying Ar-implantation doses. Normalizing the temperature-dependent PL intensities of the Ar-implanted samples to the maximum low-temperature PL intensity of the unimplanted sample A, and to the incident power density of 6.2 W cm^{-2}, yields the temperature-dependent IQE. The temperature dependence of the IQE, for the implanted samples, shows a sharp decrease with temperature, approaching zero already at low temperatures, especially for the sample with implantation dose of 1×10^{12} cm^{-2}. To avoid the contribution of parasitic defect-related emissions to the PL intensity at elevated temperatures, data points below ≈7% were dropped.

4. Conclusions

We demonstrated an experimental verification of the assumption of 100% low-temperature IQE for several efficient samples by comparing the low-temperature PL intensities. On one hand we were able to use the normalized PL intensity to assess the IQE on an absolute scale by a direct comparison. On the other hand, our results indicated that temperature-independent non-radiative losses through tunnelling seem to be a prevailing mechanism responsible for the reduced IQE in the low temperature limit. This is further confirmed by comparing the efficiencies of a sample with 100% IQE and the argon implanted samples.

Data availability statement

The data that support the findings of this study are available from the corresponding author upon reasonable request.

Acknowledgments

The authors would like to thank Dr Torsten Langer for the preparation of the Ar-implanted samples. S Sidikejiang gratefully acknowledges the support by the Braunschweig International Graduate School of Metrology (B-IGSM).

ORCID iDs

Shawutijiang Sidikejiang https://orcid.org/0000-0002-0355-3810
Andreas Hangleiter https://orcid.org/0000-0002-9183-9666

References

[1] Nakamura S, Senoh M and Mukai T 1993 High-power InGaN/GaN double-heterostructure violet light emitting diodes *Appl. Phys. Lett.* **62** 2390–2
[2] Narukawa Y, Ichikawa M, Sanga D, Sano M and Mukai T 2010 White light emitting diodes with super-high luminous efficacy *J. Phys. D: Appl. Phys.* **43** 354002
[3] Nakamura S, Senoh M, Iwasa N and Nagahama S I 1995 High-brightness InGaN blue, green and yellow light-emitting diodes with quantum well structures *Jpn. J. Appl. Phys.* **34** L797–9
[4] Fuhrmann D, Netzel C, Rossow U and Hangleiter A 2006 Optimization scheme for the quantum efficiency of GaInN-based green-light-emitting diodes *Appl. Phys. Lett.* **88** 071105
[5] Seo Im J, Kollmer H, Off J, Sohmer A, Scholz F and Hangleiter A 1998 Reduction of oscillator strength due to piezoelectric fields in GaN/$Al_xGa_{1-x}N$ quantum wells *Phys. Rev.* B **57** R9435–8
[6] Massabuau F C-P, Sahonta S-L, Trinh-Xuan L, Rhode S, Puchtler T J, Kappers M J, Humphreys C J and Oliver R A 2012 Morphological, structural and emission characterization of trench defects in InGaN/GaN quantum well structures *Appl. Phys. Lett.* **101** 212107
[7] Matthews J W and Blakeslee A E 1974 Defects in epitaxial multilayers: I. Misfit dislocations *J. Cryst. Growth* **27** 118–25
[8] Langer T, Jönen H, Kruse A, Bremers H, Rossow U and Hangleiter A 2013 Strain-induced defects as nonradiative recombination centers in green-emitting GaInN/GaN quantum well structures *Appl. Phys. Lett.* **103** 022108
[9] Hangleiter A, Fuhrmann D, Grewe M, Hitzel F, Klewer G, Lahmann S, Netzel C, Riedel N and Rossow U 2004 Towards understanding the emission efficiency of nitride quantum wells *Phys. Status Solidi* a **201** 2808–13
[10] Henry C H and Lang D V 1977 Nonradiative capture and recombination by multiphonon emission in GaAs and GaP *Phys. Rev.* B **15** 989–1016
[11] Pässler R 1978 Temperature dependences of the nonradiative multiphonon carrier capture and ejection properties of deep traps in semiconductors *Phys. Status Solidi* b **85** 203–15
[12] Landsberg P T 1991 *Recombination in Semiconductors* (Cambridge: Cambridge University Press)
[13] Yamaguchi A A, Nakano T, Sakai S, Kanitani Y and Tomiya S 2017 Carrier dynamics studies of III-nitride materials using photo-acoustic and photoluminescence measurements *Proc. SPIE* **10104** 1010409
[14] Martinez C E, Stanton N M, Kent A J, Graham D M, Dawson P, Kappers M J and Humphreys C J 2005 Determination of relative internal quantum efficiency in InGaN/GaN quantum wells *J. Appl. Phys.* **98** 053509
[15] Kazunobu K, Tomomi O, Ken-ichiro I, Yoshiki Y, Makoto S, Hirotaka I, Kenji F and Chichibu S F 2016 Determination of absolute value of quantum efficiency of radiation in high quality GaN single crystals using an integrating sphere *J. Appl. Phys.* **120** 015704
[16] Henning P, Sidikejiang S, Horenburg P, Bremers H, Rossow U and Hangleiter A 2021 Unity quantum efficiency in III-nitride quantum wells at low temperature: experimental verification by time-resolved photoluminescence *Appl. Phys. Lett.* **119** 011106
[17] Langer T, Pietscher H-G, Bremers H, Rossow U, Menzel D and Hangleiter A 2013 Nonradiative recombination due to point defects in GaInN/GaN qunntum wells induced by Ar implanation *Proc. SPIE* **8625** 862522
[18] Lasher G and Stern F 1964 Spontaneous and stimulated recombination radiation in semiconductors *Phys. Rev.* **133** A553–63
[19] Chichibu S, Azuhata T, Sota T and Nakamura S 1996 Spontaneous emission of localized excitons in InGaN single and multiquantum well structures *Appl. Phys. Lett.* **69** 4188–90
[20] Narukawa Y, Kawakami Y, Funato M, Fujita S, Fujita S and Nakamura S 1997 Role of self-formed InGaN quantum dots for exciton localization in the purple laser diode emitting at 420 nm *Appl. Phys. Lett.* **70** 981–3
[21] Langer T, Klisch M, Alexej Ketzer F, Jönen H, Bremers H, Rossow U, Meisch T, Scholz F and Hangleiter A 2016 Radiative and nonradiative recombination mechanisms in nonpolar and semipolar GaInN/GaN quantum wells *Phys. Status Solidi* b **253** 133–9
[22] Shokhovets S, Goldhahn R, Gobsch G, Piekh S, Lantier R, Rizzi A, Lebedev V and Richter W 2003 Determination of the anisotropic dielectric function for wurtzite AlN and GaN by spectroscopic ellipsometry *J. Appl. Phys.* **94** 307–12
[23] Hangleiter A, Heppel S, Off J, Kuhn F, und Scholz B, Bader S, Hahn B and Härle V 2001 Analysis of the threshold current in nitride-based lasers *J. Cryst. Growth* **230** 522–6
[24] Shen Y C, Mueller G O, Watanabe S, Gardner N F, Munkholm A and Krames M R 2007 Auger recombination in InGaN measured by photoluminescence *Appl. Phys. Lett.* **91** 141101
[25] Binder M, Nirschl A, Zeisel R, Hager T, Lugauer H-J, Sabathil M, Bougeard D, Wagner J and Galler B 2013 Identification of *nnp* and *npp* Auger recombination as significant contributor to the efficiency droop in (GaIn)N

quantum wells by visualization of hot carriers in photoluminescence *Appl. Phys. Lett.* **103** 071108
[26] Mukai T, Yamada M and Nakamura S 1999 Characteristics of InGaN-based UV/blue/green/amber/red light-emitting diodes *Jpn. J. Appl. Phys.* **38** 3976–81
[27] Piprek J 2010 Efficiency droop in nitride-based light-emitting diodes *Phys. Status Solidi* a **207** 2217–25
[28] Hader J, Moloney J V and Koch S W 2011 Temperature-dependence of the internal efficiency droop in GaN-based diodes *Appl. Phys. Lett.* **99** 181127
[29] Hecht E 2002 *Optics* (London: Pearson)
[30] Hums C, Finger T, Hempel T, Christen J, Dadgar A, Hoffmann A and Krost A 2007 Fabry–Perot effects in InGaN/GaN heterostructures on Si-substrate *J. Appl. Phys.* **101** 033113
[31] Lorenz K, Wendler E, Redondo-Cubero A, Catarino N, Chauvat M-P, Schwaiger S, Scholz F, Alves E and Ruterana P 2017 Implantation damage formation in a-, c- and m-plane GaN *Acta Mater.* **123** 177–87